

# Interface Tracking Investigation of the Sliding Bubbles Effects on Heat Transfer in the Laminar Regime

K. W. Wong, L. Bures & K. Mikityuk

To cite this article: K. W. Wong, L. Bures & K. Mikityuk (2021): Interface Tracking Investigation of the Sliding Bubbles Effects on Heat Transfer in the Laminar Regime, Nuclear Technology, DOI: [10.1080/00295450.2021.1971025](https://doi.org/10.1080/00295450.2021.1971025)

To link to this article: <https://doi.org/10.1080/00295450.2021.1971025>



Published online: 13 Nov 2021.



Submit your article to this journal 



Article views: 122



View related articles 



View Crossmark data 



# Interface Tracking Investigation of the Sliding Bubbles Effects on Heat Transfer in the Laminar Regime

K. W. Wong,<sup>a,b,c\*</sup> L. Bures,<sup>b,c</sup> and K. Mikityuk<sup>b,c</sup>

<sup>a</sup>Gesellschaft für Anlagen- und Reaktorsicherheit (GRS) gGmbH, 85748 Garching, Germany

<sup>b</sup>Paul Scherrer Institut, Nuclear Energy and Safety Section, 5232 Villigen, Switzerland

<sup>c</sup>École Polytechnique Fédérale de Lausanne, 1015 Lausanne, Switzerland

Received July 1, 2021

Accepted for Publication August 17, 2021

**Abstract** — Helium gases are utilized to remove fission products from the molten salt fast reactor (MSFR) core during operation. Helium gases and other volatile fission products may be introduced into the intermediate heat exchanger channels. The effect of these gases on heat transfer is essential for the MSFR to operate properly, especially in laminar flow regimes. The computational fluid dynamics code PSI-BOIL was selected to examine this problem because of its interface tracking capability. A periodic square duct simulation created the flow regime, resulting in a sliding bubble regime. Following that, we examined the impact of heat transfer using an extended nonperiodic channel simulation with a succession of corner bubble arrays. Due to the combined effects of low thermal diffusivity and laminar flow characteristics, it is shown that the length of heat transfer augmentation may extend to at least five bubble diameters downstream of the bubble placement. Finally, we examined the impact of interphasic heat transfer between an inert gas and a liquid. The bulk of the heat transfer amplification effect was due to the motion of the bubbles rather than interphasic heat transfer.

**Keywords** — Sliding bubbles, heat transfer, laminar flow, interface tracking simulation.

**Note** — Some figures may be in color only in the electronic version.

## I. INTRODUCTION

It is generally accepted that phase-change phenomena such as boiling result in a higher heat transfer coefficient than the single-phase convection. The increase in the heat transfer is not solely due to the phase change at the interface; the bubble dynamics are believed to have a much more crucial impact on the heat transfer enhancement than the latent heat. Cornwell<sup>1</sup> investigated the effect of bubble dynamics without phase change on heat transfer. They studied boiling phenomena over the entire tube of a shell and tube heat exchanger under constant

wall heat flux condition. The required superheat for boiling is found to be lower at the downstream side of the tube. The bubbles that originated from the phase-change process upstream of the pipe slide to the downstream position. The agitation of flow improves the immediate wall heat transfer downstream. The bubble motions induce additional fluid mixing near the wall, enhancing wall heat transfer. Thus, reducing superheat for boiling occurs downstream. The wake of the bubble can improve the near-wall heat transfer even without the occurrence of phase change. Cornwell's study set the foundation for future research on dispersed bubbly flow in the channel of the molten salt fast reactor (MSFR) heat exchanger. In the MSFR, there is some gaseous content inside the fuel

\*E-mail: [kinwing.wong@grs.de](mailto:kinwing.wong@grs.de)

salt, such as helium and other volatile fission products. Even though the gaseous component of the fuel salt is relatively modest (1% or 2%), the bubbles influence near-wall heat transfer by sliding against the wall or disrupting the boundary layer. Experiments with sliding bubbles were also conducted, and the cooling plume's existence was confirmed in water.<sup>2</sup> Donoghue et al. also discovered an increase in heat transfer due to bouncing bubble motions,<sup>3</sup> similar to sliding bubbles. However, only a few studies have used computational fluid dynamics (CFD) to examine the effect of bubble dynamics on heat transfer.<sup>4–6</sup> Kim and Lee simulated the effect of surface wettability on heat transfer using the Volume of Fluid model (VOF) with contact angle modeling.<sup>6</sup> In their study, both hydrophilic and hydrophobic surfaces were studied (i.e., for equilibrium contact angles from 10 to 170 deg). If the advancing and receding contact angles are known, then the surface tension force attributed by the difference between advancing and receding contact angles can contribute to the effects of bubbles adhering or detaching from the wall (in terms of wall adhesive force directions). The authors also discussed that the surface heat transfer improves in both hydrophilic and hydrophobic surfaces [i.e., bubble bouncing (contact angle smaller than 60 deg)] and surface contacting regime (i.e., contact angle greater than 120 deg) and that the surface contacting regime provides the most significant heat transfer enhancement. In a recent study,<sup>7</sup> the authors continued with the previous investigation on VOF with a dynamic contact angle model<sup>8</sup> and concluded that the increase of heat transfer is strongly correlated with the skin friction and the deformability of the bubble. The model has also been applied to the flow boiling phenomenon in mini channels, considering the surface effects and inertia. Apart from these researches directly related to the surface effects, others also investigated adiabatic bubbly flow conditions in a bare channel using interface tracking Direct Numerical Simulation (DNS) (Refs. 9 and 10). The interface tracking simulation has been successfully applied in other situations involving complex bubble dynamics, including deformation and collision dynamics,<sup>11</sup> bubble population effects in the pressurized water reactor channel,<sup>12</sup> and nucleate boiling.<sup>13</sup> Thus, the interface tracking technique is deemed suitable for studying the macroscopic impact of inert gas on laminar heat transfer.

This study consists of three tasks:

1. *Determine the flow regime.* Usui and Sato<sup>14</sup> discovered void “coring” behavior for spherical bubbles. They reported that the bubbles would cling to the wall

if the bubbles were distorted. However, no investigations have shown that this phenomenon occurs in mini channels (less than 5 mm).<sup>15</sup> Therefore, the relevant flow regime was investigated using a 2-mm-square channel.

2. *Modify the interface tracking solver.* Due to the absence of interphasic heat transfer between the inert gas and the molten salt, the existence of the interface provides no feedback on the temperature field. Since the primary purpose of the CFD Code PSI-BOIL is to model gas-liquid phase transitions or diabatic phenomena, the interfacial temperature is always maintained at saturation temperature as a boundary condition. The two-phase energy solver is modified to update the interfacial temperature in response to the surrounding liquid temperature as if it were a moving bluff object inside the flow.

3. *Investigate the effect of the bubbles' motion to the temperature field at the near-wall region.* Bubbles in the flow channel serve as bluff bodies. When the flow passes around the bubble, the near-wall boundary layer will be perturbed, thus enhancing wall heat transfer. Interface tracking simulations are performed to investigate these effects.

## II. NUMERICAL MODEL

### II.A. Governing Equation and the CFD Code PSI-BOIL

For reference, the relevant governing equations for continuity, momentum, and energy fields are as follows:

$$\cdot \mathbf{u} = 0 , \quad (1)$$

$$\frac{\partial \rho \mathbf{u}}{\partial t} + \cdot (\rho \mathbf{u} \mathbf{u}) = - p + \rho g + \cdot [\mu (\mathbf{u} + \mathbf{u}^T)] + \sigma \kappa \delta_s \mathbf{n} , \quad (2)$$

and

$$\frac{\partial \rho c_p T}{\partial t} + \cdot (\rho c_p \mathbf{u} T) = \cdot (\lambda T) + Q . \quad (3)$$

A color function is employed as an indicator for tracking the interfacial position by solving the color advection equation:

$$\frac{\partial \phi}{\partial t} + \mathbf{u} \cdot \nabla \phi = 0 . \quad (4)$$

A review of different interface tracking methods can be found in Ref. 16. The interface sharpening equation is solved after each advection step to guarantee the

sharpness of the interface in the PSI-BOIL. The sharpening operation can be found in Ref. 17. PSI-BOIL is an open-sourced CFD code developed at the Paul Scherrer Institute. It is an acronym for Parallelized for Boiling Phenomenon and is primarily aimed at fundamental research on phase-change phenomena. PSI-BOIL is a fully three-dimensional and parallelized finite volume code for incompressible flows. The governing equations solved in the PSI-BOIL are based on a single fluid formulation; the cell density is computed using the arithmetic average of the liquid and vapor properties. In addition, a surface tension component is included in the momentum equation to account for the pressure difference between the vapor and liquid boundaries [as shown in Eq. (2)]. PSI-BOIL uses the projection step method to solve the momentum equation (time-stepping scheme). The interface is monitored using the Constrained Interpolation Profile – Conservative Semi-Lagrangian second-order method or CIPCSL-2; each step additionally solves the color advection equation. The developed

algorithm is detailed in Ref. 17. The phase-change module of the code was omitted from this study due to the absence of phase change.

## II.B. Modification of the Treatment for Interface Temperature

The original solver maintained the interfacial temperature at saturation. The method is well suited for mimicking phase change. In the current study, interfacial exchanges in mass and heat transfer are irrelevant. This implies that the temperature field will retain a temperature consistent with the neighboring phase regardless of the presence or absence of the interface. The temperature field is entirely determined by convection. The adiabatic interface assumption, on the other hand, prohibits heat transfer over the interface. In the temperature field, the interface behaves as a bluff body. A zero-temperature gradient (i.e., Neumann condition) should be applied to the interface cell. Because the interface temperature is

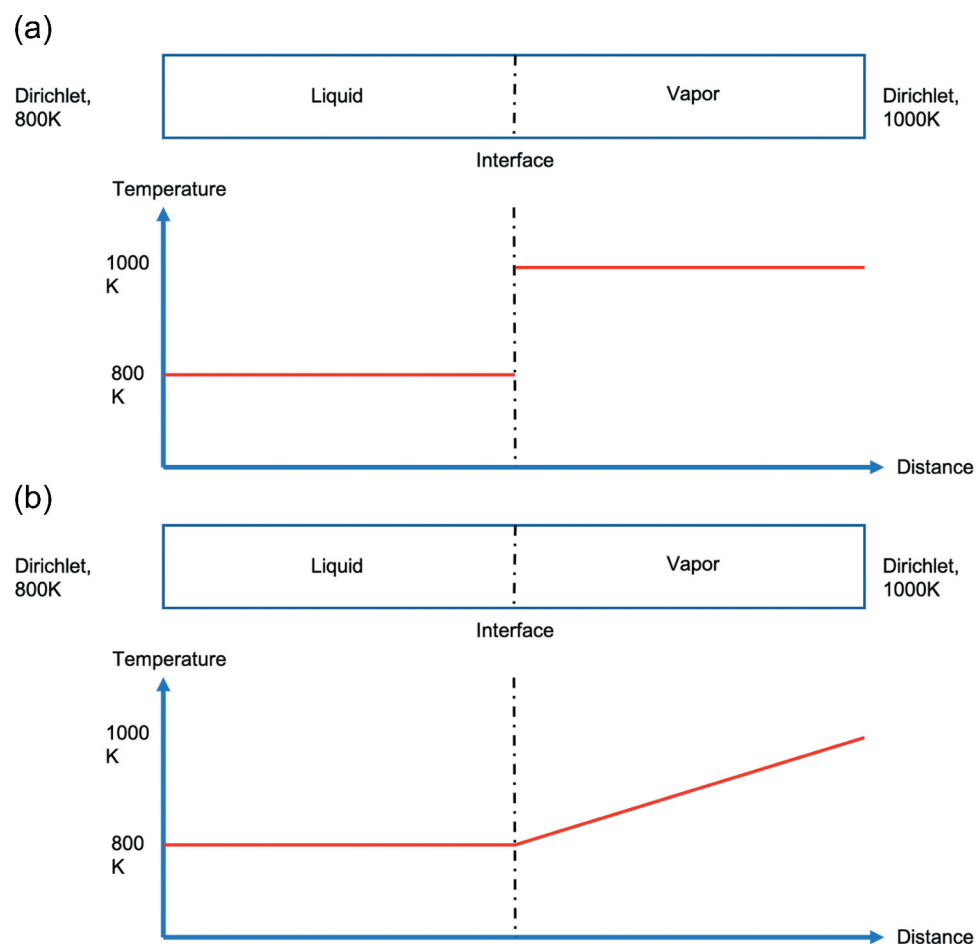


Fig. 1. Modification of the interface temperature: (a) disconnection of the information between liquid and vapor cells and (b) extrapolation step.

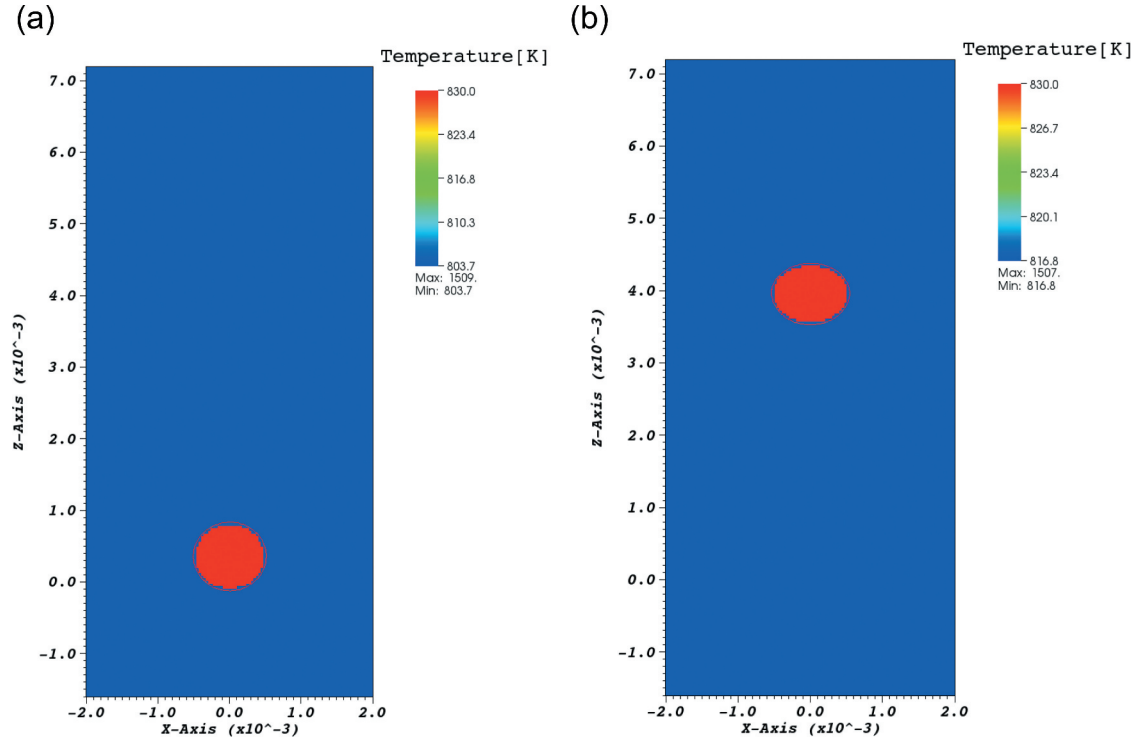


Fig. 2. Temperature field at the (a) initial and (b) end of the rising period. The red contour represents the liquid-vapor interface.

TABLE I  
Summary of the Physical Properties Used for Both Salts and Inert Gas

	$c_p$ (J/Kg·K)	$\rho$ (kg/m <sup>3</sup> )	$\mu$ (kg/m <sup>-1</sup> s <sup>-1</sup> )	$\lambda$ (W/m · K)	Pr
Salt 1	4039.82	4039.82	0.00714	1.0	29
Salt 2	2414.17	1940.0	0.0056	1.0	13
Inert gas	5206.0	0.3101	$7.81 \cdot 10^{-5}$	0.53	0.77

not maintained constant, the interfacial temperature can only be estimated using the information from neighboring cells (i.e., saturation temperature in the past). Temperature extrapolating from the gradient of the non-interface cell, the interface temperature can be set using information from color functions for nearby interfacial cells. Consider the case where the interface is located

between cells  $i$  and  $i + 1$ . Suppose the color function of cell  $i$  is greater than or equal to 0.5 (indicating a liquid state). In that case, cell  $i + 1$  must be a gas cell (i.e., color function smaller than 0.5). Thus, an extrapolation equation can be used to predict the interfacial temperature:

$$T_{int} = T_l + \frac{\partial T}{\partial x'} \delta x', \quad (5)$$

TABLE II  
Mesh Sensitivity Analysis on Local Void Fraction

	$a_{-0.25mm}$	$a_{+0.25mm}$
$72 \times 72 \times 288$	0.947	0.892
$96 \times 96 \times 384$	0.937	0.911
$120 \times 120 \times 480$	0.931	0.923

where  $T_l$  represents the temperature of the liquid cell, and  $x'$  represents the distance between the liquid cell and the interface. Figure 1 illustrates the modification of the temperature solver by using a one-dimensional channel with Dirichlet boundary condition on both sides.

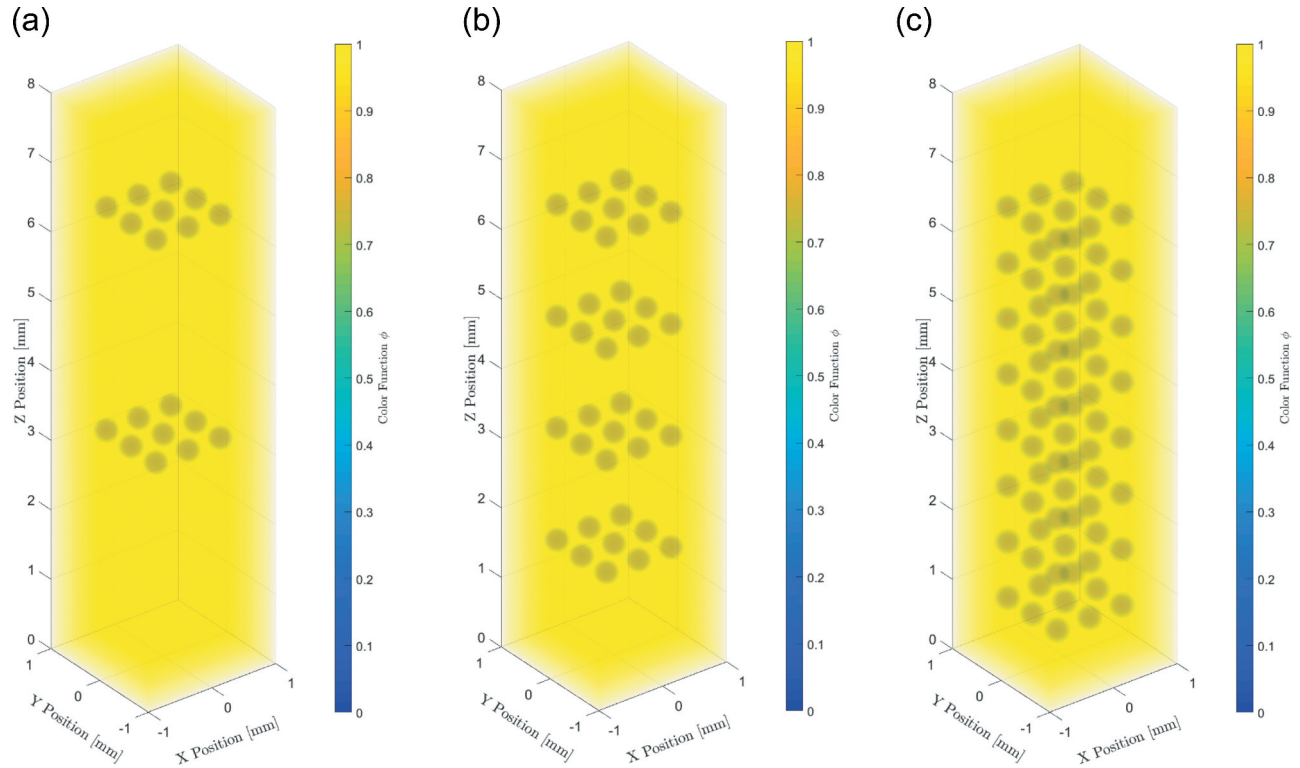


Fig. 3. Initial color function for the three periodic simulations: (a) 18 bubbles, (b) 36 bubbles, and (c) 72 bubbles.

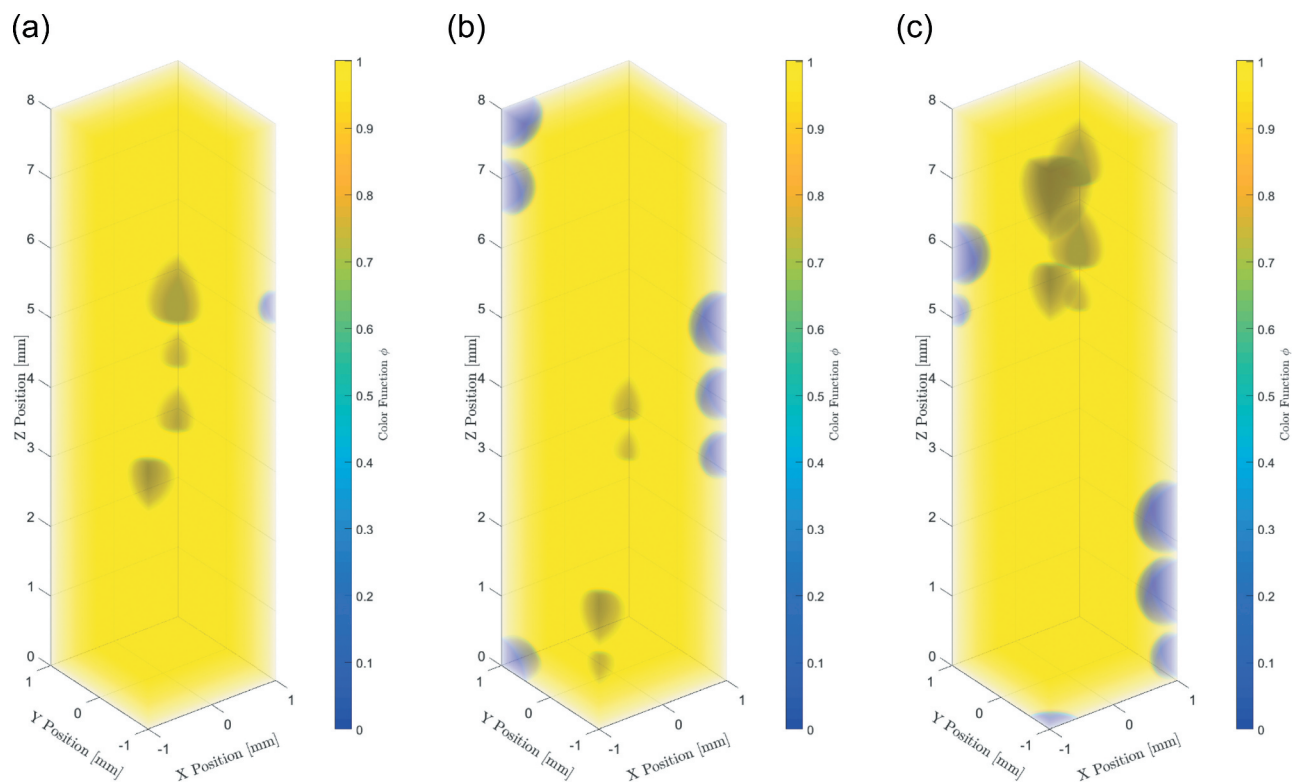


Fig. 4. Quasi-steady color function for the three periodic simulations: (a) 18 bubbles, (b) 36 bubbles, and (c) 72 bubbles.

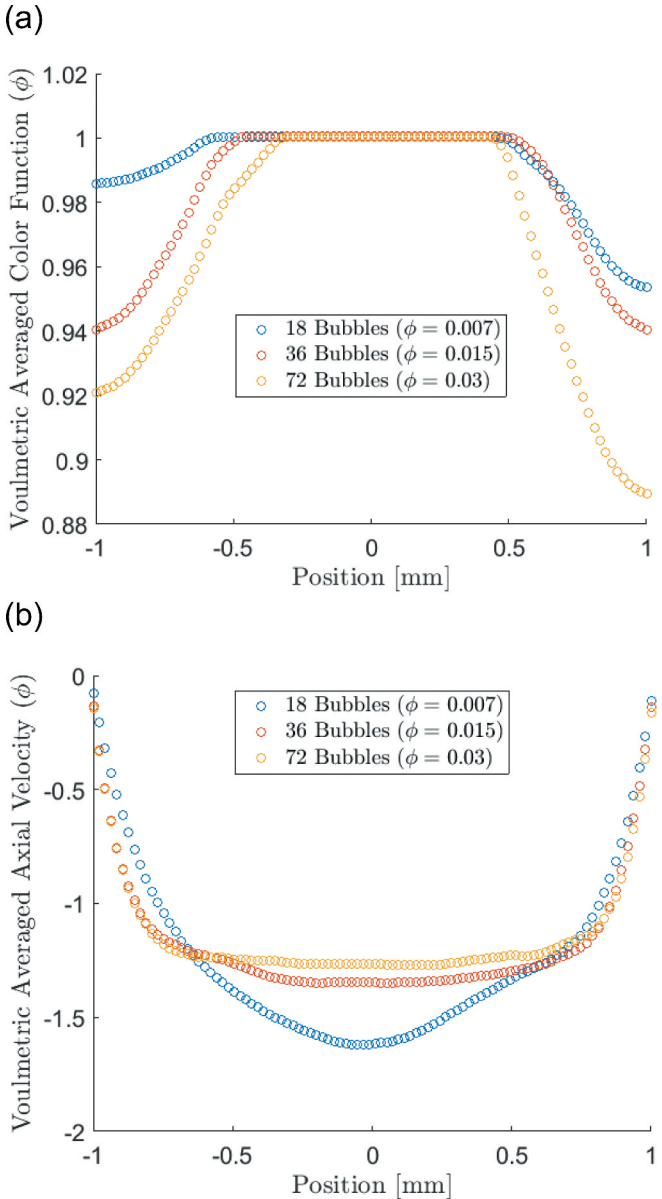


Fig. 5. Volumetric-averaged data for the periodic simulation with void fraction of 0.7%, 1.5%, and 3.0%: (a) volumetric-averaged color function and (b) volumetric-averaged velocity profile.

### II.B.1. Simple Test for the Modification

Within the internally heated liquid, a molten salt bubble is immersed at an initial temperature of 800 K. Then, the bubble rises with buoyancy due to the density difference between the liquid and vapor phases. For the temperature field, the interface temperature is the same as the liquid temperature  $T_l$  since temperature extrapolation was conducted after each step from the liquid to the vapor cell. The temperatures before and after are shown in

Fig. 2. There is a temperature differential of about 2 to 20 mK between the interface and liquid cells.

## III. BUBBLE BEHAVIOR IN SQUARE CHANNEL

### III.A. Physical Properties

This study used the following values of the LiF-ThF<sub>4</sub>, LiF-BeF<sub>2</sub>, and helium gas properties to simulate two postulated molten salts. The surface tension and contact angles were  $22.8 \cdot 10^{-2}$  Nm and 90 deg, respectively. The 90 deg of contact angle does not represent the expected value of the considered molten salt; however, it also depends on the material's surface, which is a limitation for the current study. In PSI-BOIL, the equilibrium contact angle (i.e., the contact angle measured at rest) is used to compute the interface normal at the wall boundary.<sup>18</sup> Other values for the equilibrium contact angle can be studied, or even a dynamic contact angle model<sup>8,19,20</sup> can be adopted to simulate the effect of surface wettability. The specific heat capacity of LiF-ThF<sub>4</sub> used in this study is greater than the instance described in Refs. 21 and 22 to compare the effect of thermal diffusivity. The specific heat capacity formula in Ref. 21 yields a value of 1723.9 J/Kg·K. If the lower specific heat capacity value is utilized, the Prandtl number (Pr) of LiF-ThF<sub>4</sub> would be comparable to that of LiF-BeF<sub>2</sub>. As a result, the second postulated salt uses the elevated value for specific heat to investigate the impact of the Pr number on heat transport. A summary of the two salts and helium gas is listed in Table I.

### III.B. Determination of the Flow Regime

The impact of the flow regime within the mini channel on heat transfer is particularly significant to the study; for example, the response of the sliding bubble regime on the wall and the void coring regime has a fundamental difference in influencing heat transfer behavior. The whole domain is  $2 \times 2 \times 8$  mm<sup>3</sup> ( $L_x \times L_y \times L_z$ ) in size. Except for the top and bottom sides of the domain (i.e., the  $\pm z$  direction), are periodic, the remaining sides are set as wall boundaries (non-periodic). From mesh sensitivity analysis, the result is dependent only on the orthogonal direction (i.e.,  $x - y$  direction), but not the axial direction. For this calculation, 72, 96, and 120 cell sizes were tested (see Table II on void fraction results), and it was found that 96 cells were adequate (i.e., at least 14 cells across the bubbles with  $D_B$  of 0.3 mm) for the current calculation without phase change. Therefore, the

mesh size is set at  $96 \times 96 \times 384$  for the subsequent discussions.

According to Ref. 23, the equilibrium void fraction is about 1%. This value is chosen as the boundary condition for the periodic simulation (i.e., the total void fraction  $\alpha$  is around 0.01), and three initial bubble distributions (i.e., in Fig. 3 a postulated initial bubble diameter  $D_B$  of 0.3 mm was used to investigate the interaction between the wall and tiny bubbles in this study) were selected to mimic the impact of void percent on the quasi-static bubble distribution.

A pressure gradient  $\Delta p$  of  $2 \times 10^5$  Pa was selected to correspond to the fully developed velocity profile of about  $1 \text{ ms}^{-1}$ . The bubbles coalesced near the center for early time steps (i.e., void coring). They then drifted toward the wall after being severely distorted. Figure 4 illustrates the quasi-static bubble distributions for these instances with a simulation duration of 0.1 s.

It is possible to run a more extended simulation. The bubbles will continue to merge until only four bubbles are remaining at the channel's corners. The leading cause for the drift toward the corner is a flow arrangement typical of square ducts. In the laboratory frame, the corner of the square duct has the lowest velocity. This also implies a greater velocity in terms of bubble coordinates so that bubbles drift to the corner. Additionally, similar sliding bubble behavior is anticipated in channels with internal corners, such as semicircular channels. However, the result shown in this section assumes a 90-deg contact angle. The larger bubble migrates to the center for vertically upward flow in large tubes (i.e.,  $D_B > 10$  mm). The smaller bubble migrates to the wall and vice versa for downward flow. The

bubble migrates because of the lateral force acting on it in a sheared velocity field. Tomiyama et al.<sup>24</sup> offered experimental evidence for the previous assertion, saying that two regimes depending on the size of the bubble control its migratory orientation. A larger-sized bubble deforms more than a smaller bubble. This is reflected in the Eotvos/Bond ratio, which for large diameter bubbles is about 4 to 5. As a result, bubbles tend to migrate toward the wall in our simulations. In molten salt, the Eotvos/Bond ratio is considerably lower than in Tomiyama et al.'s experiment. Additionally, the low Eotvos/Bond ratio shows that the flow is unaffected by buoyancy because of its high surface tension. Another piece of evidence is that the vapor bubbles that migrated from the nucleation site on the heated surface to the flow's center slid over the wall rather than toward the flow's center.<sup>16</sup> Except for the flow direction, the flow arrangement is almost identical to our periodic simulation. Lu et al.<sup>9</sup> stated that DNS results were obtained using a fluid with a density difference between the liquid and vapor of 10 and an Eotvos/Bond number of 0.5 in a laminar flow arrangement; however, the surface tension of the liquid was maintained very high, and deformation/coalescence was ignored. They found that bubbles indeed move toward the channel's center, although in the opposite direction as the liquid.

Using a volumetric-averaged color function and velocity profile, Fig. 5 depicts the bubble channel's quasi-steady behavior. According to the average color function, the original bubble distribution was distributed onto the four corners of the channel. As a result, the volumetric-averaged profile showed dips on both sides of the channel. The larger the initial void percentage, the deeper

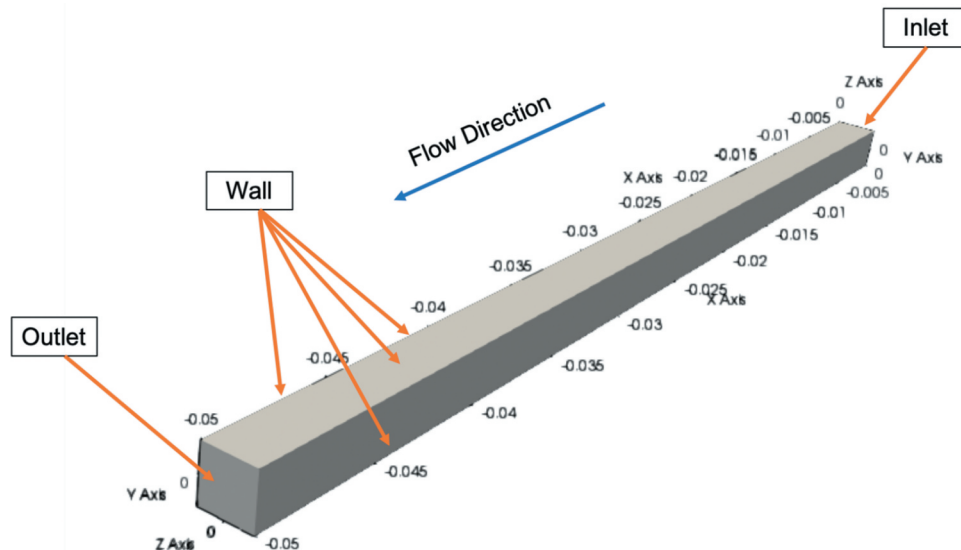


Fig. 6. Domain specification for adiabatic bubbly flow simulation.

TABLE III

Mesh Sensitivity Analysis on Heat Transfer Enhancement Ratio

	$\max(r_h)$	$r_h$ (0.045 m)
72 × 72 × 1800	3.57	1.21
96 × 96 × 2400	4.13	1.37
120 × 120 × 3000	4.35	1.48

the dip at the channel's boundaries will be. The void fraction influences the variations in the velocity profile. The wake structure produced by the bubbles cannot affect the whole channel for a tiny void fraction (i.e., less than 0.001). (That is, the profile is similar to the one for a fully developed laminar velocity profile.) The shift in the velocity distribution begins to create the plug flow profile for a higher void percentage of approximately 0.015. It means that the bubbles' wake structures start to disturb the boundary layer. Even though the averaged Reynolds number ( $Re$ ) was considerably lower than the transitional  $Re$  for duct flow, the disruption causes the velocity profile to resemble a turbulent profile.

#### IV. EFFECTS ON HEAT TRANSFER

This section aims to investigate the relationship between the  $Pr$  number and the heat transfer enhancement ratio. To examine the influence on the  $Pr$  number, two simulations were carried out: one with a single group of

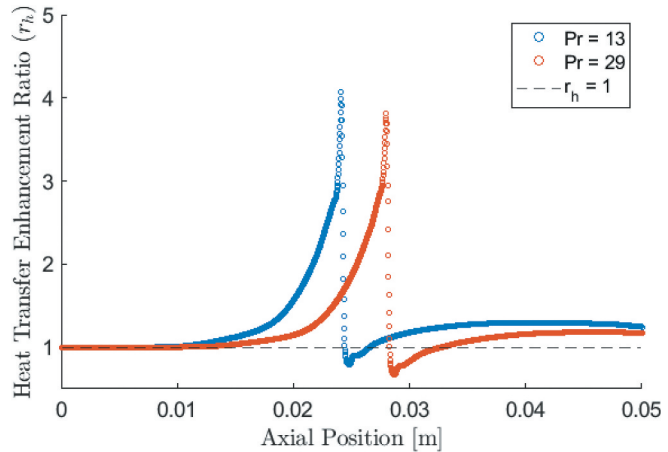


Fig. 7. Heat transfer enhancement ratio for a single bunch of sliding bubbles.

sliding bubbles and another with four groups of sliding bubbles.

##### IV.A. Simulation Setup

A square duct domain  $500 \times 2 \times 2$  mm in size was built. Figure 6 illustrates the domain definition for the bubbly flow simulation as well as the boundary conditions used. The domain's mesh size is set at  $96 \times 96 \times 2400$ .

The radius of the bubbles was chosen to be in the submillimeter range (i.e., bubble diameter = 0.3 mm). To assess the heat transfer enhancement caused by bubble motions, a standard bubble array of 36 bubbles was

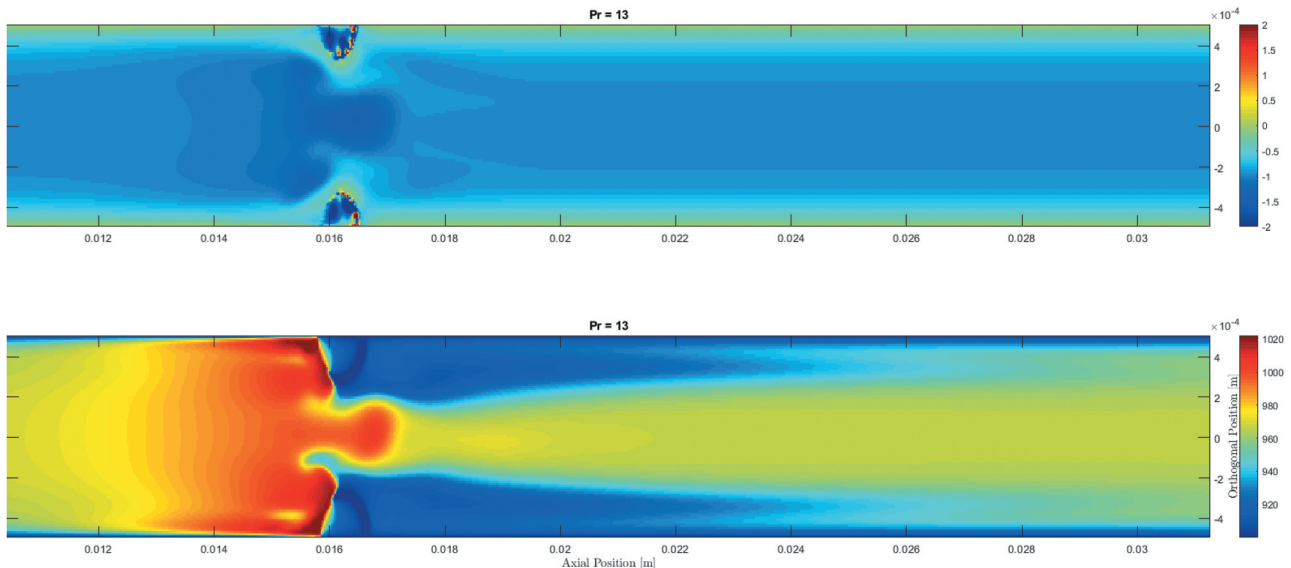


Fig. 8. Velocity and temperature slice for corner bubble array for salt with  $Pr = 13$ . The figure shows the orthogonal cross section of the square duct. The horizontal and vertical axis represents the axial and orthogonal directions of the flow.

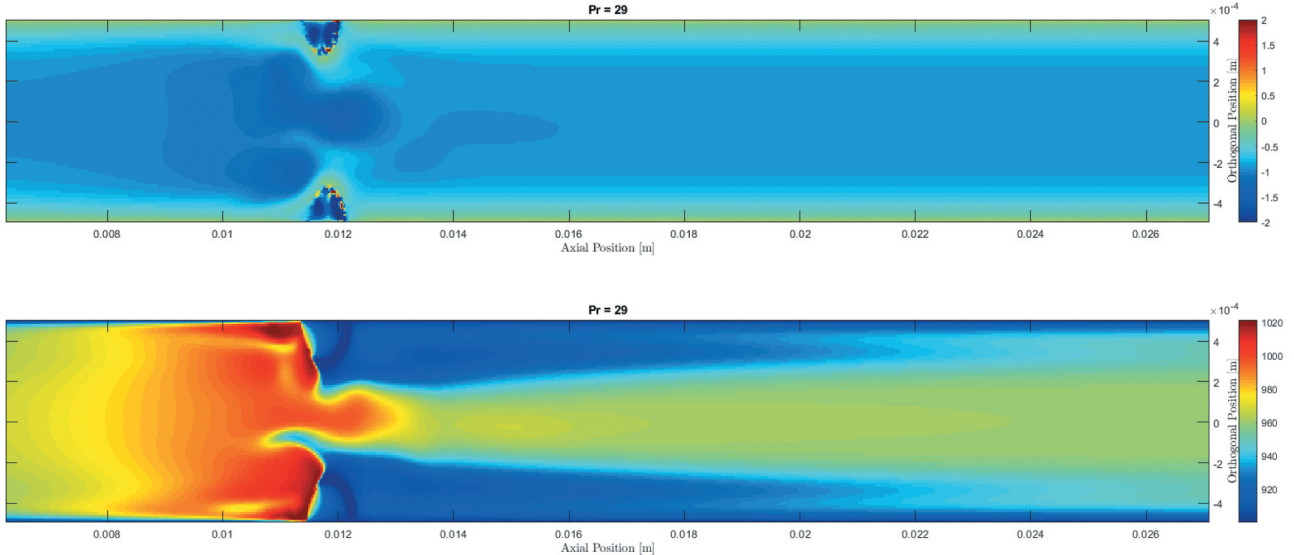


Fig. 9. Velocity and temperature slice for corner bubble array for salt with  $\text{Pr} = 29$ . The figure shows the orthogonal cross section of the square duct. The horizontal and vertical axis represents the axial and orthogonal directions of the flow.

started in the channel's inlet region. This setup is intended to mimic the first phase of bubble injection into the heat exchanger channel before the bubbles attain a quasi-static state. According to the findings of the periodic simulation, the bubbles migrate to the rectangular duct's four corners. These data were used as the boundary condition for a channel simulation to investigate the effect of heat transfer produced by bubbles traveling along the four edges. At the channel's entrance, bubbles were generated in four unique axial locations (i.e., 0.05, 0.10, 0.15, and  $0.20L_x$ ) and four distinct axial positions (i.e., the flow was moving in the  $x$ -direction).

#### IV.B. Heat Transfer Enhancement Ratio

To quantify the impact of the bubble on heat transfer, the heat transfer enhancement ratio  $r_h$ , which is the ratio of the heat transfer coefficient of the sliding bubble regime over the single-phase condition, was employed to reflect the augmentation effect of heat transfer in the absence of inert gas. For comparison, a single-phase calculation with the same mesh size was simulated and used as the reference (i.e., the fully developed value).

#### IV.C. Single Group of Corner Bubbles Test

A single group of corner bubbles is employed as a preliminary test to evaluate its effect on heat transfer. To check the mesh sensitivity of the reported results, three numerical solutions of the three mesh size settings (i.e.,  $72 \times 72 \times 1800$ ,  $96 \times 96 \times 2400$ , and  $120 \times$

$3000$ ) are checked with the maximum value of  $r_h$  and the value at 0.045 m (see Table III). The case with 96 cells yields reliable results that are sufficient for the subsequent discussions.

To determine the impact of the  $\text{Pr}$ , both fluids are simulated using the computational domain described earlier and compared to single-phase simulations. The direct comparison of the heat transfer enhancement ratio between two salts with varying  $\text{Pr}$  is shown in Fig. 7. The enhancement of heat transfer began upstream of the bubble. It rapidly diminished downstream due to the stalling of fluid mixing in the bubble's immediate vicinity. The difference between the two salts in terms of immediate increase of heat transfer at the bubble location is negligible. This indicates that the velocity perturbation, controlled by the bubble

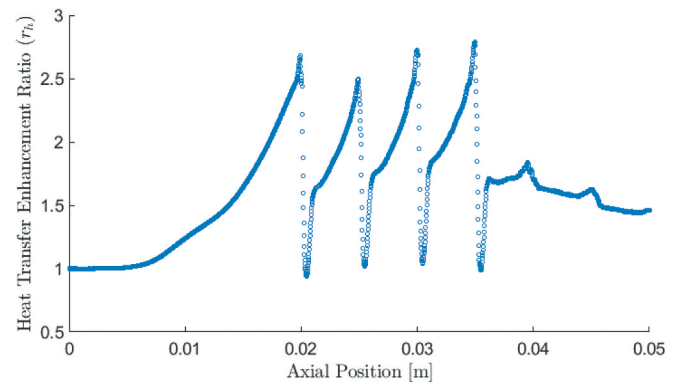


Fig. 10. Heat transfer enhancement ratio for multiple bunches of sliding bubbles.

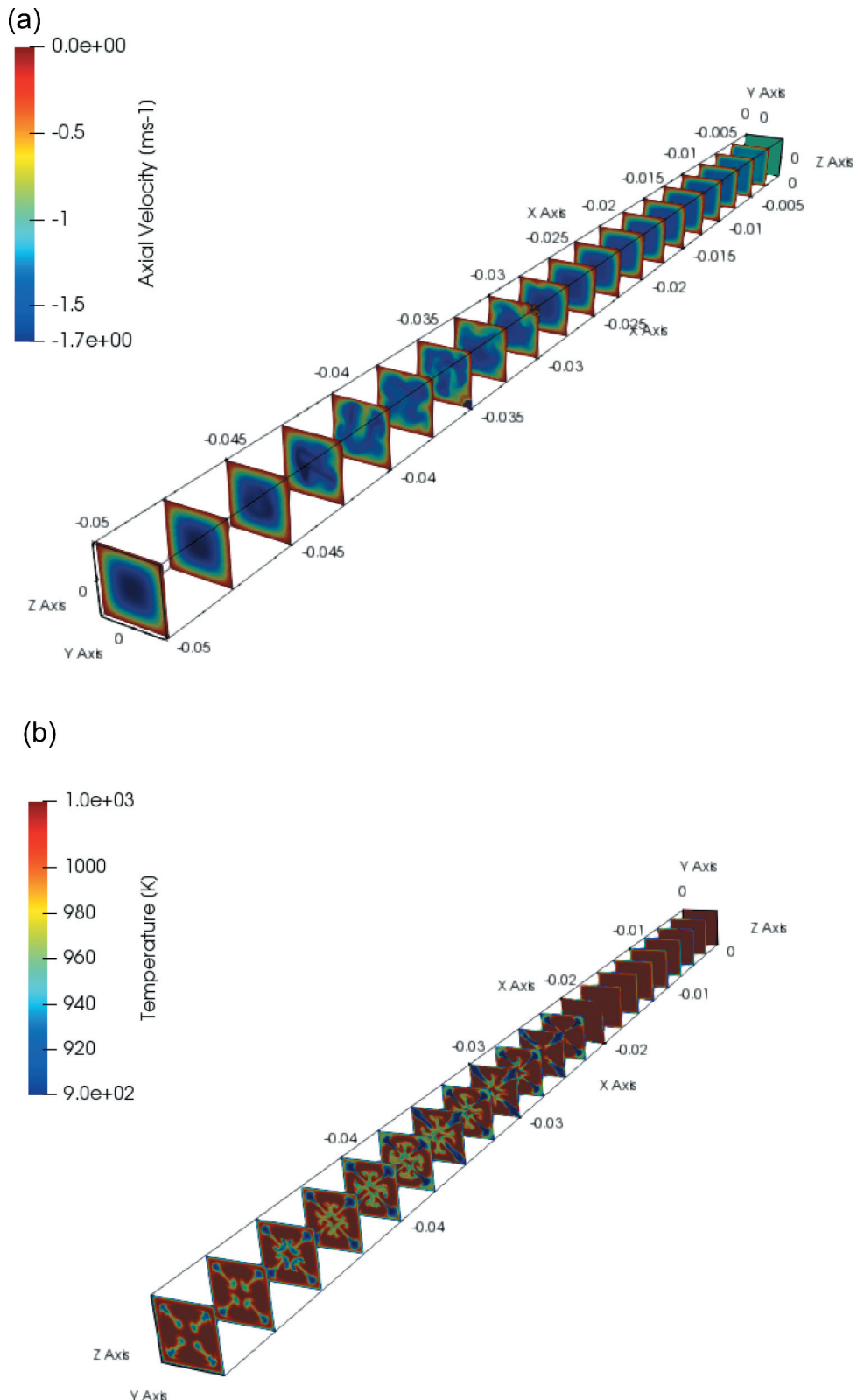


Fig. 11. Axial slices for perturbation in (a) velocity and (b) temperature field.

size, is the primary driver of the increase. Due to the laminar flow characteristic, the temperature perturbation extends for multiple bubble diameters. It improves the downstream location's heat transfer. This combines with the effect of low thermal diffusivity of molten salt, leading to extended heat transfer augmentation. The extent of velocity and temperature perturbations can be seen in Figs. 8 and 9. Due to the absence of the following increase in heat transfer for a single cluster of corner bubbles, the effect of  $\text{Pr}$  cannot be seen clearly, despite some variations in the length of the temperature wake.

#### IV.D. Multiple Group of Corner Bubbles Test

Four distinct groups of corner bubbles are analyzed in the same way. Figure 10 shows the  $r_h$  for the scenario with four corner bubble arrays. The initial increase in  $r_h$  occurs because of the bubbles disturbing the boundary layer, as stated in Sec. IV.C. The temperature field is less diffusive than the velocity/momentum field in high  $\text{Pr}$  liquids such as molten salt. As shown in Fig. 11, the velocity flows from left to right, and the disturbance occurs mainly before and around the bubbles. It is also worth noticing that the disruption subsides after a few bubble diameters. This, however, would be completely different, as shown in the temperature field. There are two observations: First, the temperature perturbed region is very long, lasting at least five bubble diameters; and second, even after the temperature perturbation, the temperature field retained the state shown in the end region of Fig. 11. This effect leads to an increase in heat transfer even at five bubble sizes. The effect is partially due to the large  $\text{Pr}$  number of the molten salt, but the bulk of the effect is due to the laminar flow regime. Because the momentum field is more diffusive than the temperature field, the velocity field was restored to laminar flow before the temperature was diffused throughout the channel. One of the features of laminar flow is that the flow is streamlined and the temperature does not mix, resulting in a frozen temperature perturbation and enhanced heat transfer effect even after a few bubble diameters.

Figure 12 illustrates the comparison for both salts. The identical heat transfer augmentation procedure was performed, as can be observed. It had a high heat transfer enhancement ratio upstream of the bubble. However, the temperature perturbation was frozen due to the simulation's laminar velocity profile downstream. The combined impact of the  $\text{Pr}$  number and the laminar velocity profile ensure that the heat transfer coefficient downstream of those bubbles is effectively increased.

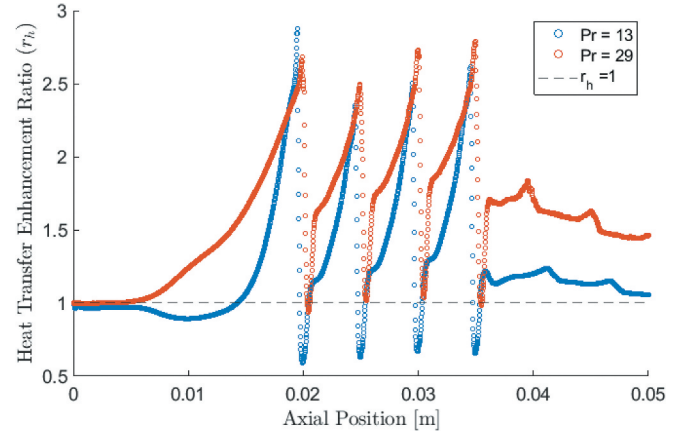


Fig. 12. Heat transfer enhancement ratio for multiple bunches of sliding bubbles.

#### IV.E. Effects of Interphasic Heat Transfer

In Secs. IV.A through IV.D, the heat transfer between the molten salt and the inert gas was neglected by modifying the solver inside the PSI-BOIL. This allowed us to focus only on the effect due to velocity perturbation. Now, the heat transfer between two phases is considered by using the single-phase solver in PSI-BOIL (i.e., it solves the enthalpy equation, however, without considering the interface between the two phases). Therefore, the interphasic heat transfer is simulated with the bubble effects by conduction between two phases. Figure 13 compares the heat transfer enhancement ratio of the cases of not simulating and simulating the interphasic heat transfer. It is found that the  $r_h$  is higher for the case with interphasic heat transfer, the reason is that the high thermal diffusivity of the helium gas has a relatively high specific heat capacity and thermal conductivity. Therefore, the interphasic heat transfer promotes the temperature mixing and the effect due to the bubble motion. The region following the last bubble

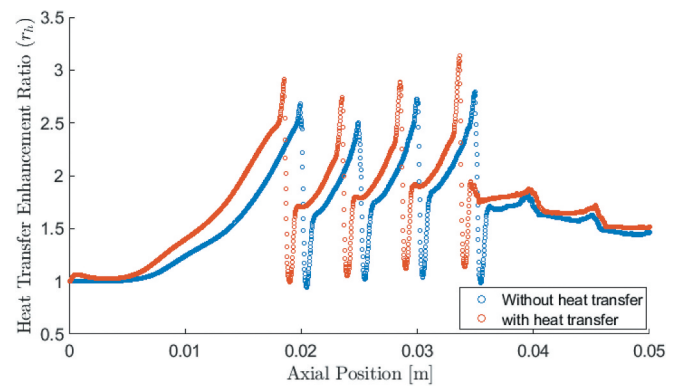


Fig. 13. Comparison of the effects for interfacial heat transfer.

is similar for both cases. There is no helium bubble, therefore, no influence due to the interphasic heat transfer. Due to the nature of heat transfer enhancement, the more bubbles upstream, the more chaotic would be the temperature downstream, and thus resulting in a higher  $r_h$  downstream. The result shown here is not restricted only to molten salt liquid but also applies to other fluid systems, like air-water flow, as the implication is similar for the wall characteristic with a 90-deg contact angle.

## V. CONCLUSION

With an interface tracking simulation code it is possible to simulate the effect to heat transfer due to the bubble motion. The current study focused on a specialized condition filled with molten salt and helium gases with a 90-deg contact angle. From the analysis, the attachment of the inert gases on the wall improves the heat transfer in the laminar regime. The interphasic heat transfer and bubble motion on the agitation of heat transfer have been separated in numerical simulation. The effect of bubble motion was found to have a significant effect on heat transfer, which coincides with the findings in other experimental literature.

## Acknowledgments

The simulations were run on the ETH Zürich and Paul Scherrer Institute's Euler and Merlin clusters. This research received no external research funding.

## ORCID

K. W. Wong  <http://orcid.org/0000-0002-7577-8736>

## References

1. K. CORNWELL, "The Influence of Bubbly Flow on Boiling from a Tube in a Bundle," *Int. J. Heat Mass Transfer*, **33**, 12, 2579 (1990); [https://doi.org/10.1016/0017-9310\(90\)90193-X](https://doi.org/10.1016/0017-9310(90)90193-X).
2. O. MEEHAN et al., "Forced Convection in the Wakes of Sliding Bubbles," *J. Phys. Conf. Series*, **745**, 32117 (Sep. 2016); <https://doi.org/10.1088/1742-6596/745/3/032117>.
3. D. B. DONOGHUE et al., "Bouncing Bubble Dynamics and Associated Enhancement of Heat Transfer," *J. Phys. Conf. Series*, **395**, 12167 (Nov. 2012); <https://doi.org/10.1088/1742-6596/395/1/012167>.
4. K. E. ALBAHLOUL et al., "Comparing the Enhancement of Heat Transfer Caused by Sliding Gas Bubbles and by Sliding Vapor Bubbles in Subcooled Flow in a Minichannel," *Proc. ASME 2013 Heat Transfer Summer Conf. collocated with the ASME 2013 7th Int. Conf. on Energy Sustainability and the ASME 2013 11th Int. Conf. on Fuel Cell Science, Engineering and Technology*, Minneapolis, Minnesota, Vol. 2: Heat Transfer Enhancement for Practical Applications; Heat and Mass Transfer in Fire and Combustion; Heat Transfer in Multiphase Systems; Heat and Mass Transfer in Biotechnology, p. V002T07A042 (July 2013); <https://doi.org/10.1115/HT2013-17070>.
5. J. R. WILLARD and D. K. HOLLINGSWORTH, "Numerical Investigation of Heat Transfer in the Wake of a Single Highly Confined Bubble in a Horizontal Minichannel," *Proc. ASME 2018 16th Int. Conf. on Nanochannels, Microchannels, and Minichannels*, Dubrovnik, Croatia, June 10–13, 2018, Vol. 51197, p. V001T02A014 (2018); <https://doi.org/10.1115/ICNMM2018-7693>.
6. J. KIM and J. S. LEE, "Surface-Wettability-Induced Sliding Bubble Dynamics and Its Effects on Convective Heat Transfer," *Appl. Thermal Eng.*, **113**, 639 (Feb. 2017); <https://doi.org/10.1016/j.applthermaleng.2016.11.097>.
7. J. KIM and J. S. LEE, "Effects of Surface Tension and Inclined Surface Wettability on Sliding Bubble Heat Transfer," *Int. J. Thermal Sci.*, **142**, 77 (2019); <https://doi.org/10.1016/j.ijthermalsci.2019.04.013>.
8. K. YOKOI et al., "Numerical Studies of the Influence of the Dynamic Contact Angle on a Droplet Impacting on a Dry Surface," *Phys. Fluids*, **21**, 7, 072102 (July 2009); <https://doi.org/10.1063/1.3158468>.
9. J. LU, S. BISWAS, and G. TRYGGVASON, "A DNS Study of Laminar Bubbly Flows in a Vertical Channel," *Int. J. Multiphase Flow*, **32**, 6, 643 (June 2006); <https://doi.org/10.1016/j.ijmultiphaseflow.2006.02.003>.
10. L. WEI et al., "Numerical Study of Adiabatic Two-Phase Flow Patterns in Vertical Rectangular Narrow Channels," *Appl. Thermal Eng.*, **110**, 1101 (Jan. 2017); <https://doi.org/10.1016/j.applthermaleng.2016.09.007>.
11. Y. FAN, J. FANG, and I. BOLOTNOV, "Complex Bubble Deformation and Break-Up Dynamics Studies Using Interface Capturing Approach," *Experiment. Comput. Multiphase Flow*, **3** (July 2020); <https://doi.org/10.1007/s42757-020-0073-3>.
12. J. CAMBARERI, J. FANG, and I. BOLOTNOV, "Interface Capturing Simulations of Bubble Population Effects in PWR Subchannels," *Nucl. Eng. Des.*, **365**, 110709 (Aug. 2020); <https://doi.org/10.1016/j.nucengdes.2020.110709>.
13. M. LI, J. MOORTGAT, and I. BOLOTNOV, "Nucleate Boiling Simulation Using Interface Tracking Method," *Nucl. Eng. Des.*, **369**, 110813 (Dec. 2020); <https://doi.org/10.1016/j.nucengdes.2020.110813>.

14. K. USUI and K. SATO, "Vertically Downward Two-Phase Flow, (I): Void Distribution and Average Void Fraction," *J. Nucl. Sci. Technol.*, **26**, 7, 670 (July 1989); <https://doi.org/10.1080/18811248.1989.9734366>.
15. H. IDE, A. KARIYASAKI, and T. FUKANO, "Fundamental Data on the Gas-Liquid Two-Phase Flow in Minichannels," *Int. J. Thermal Sci.*, **46**, 6, 519 (June 2007); <https://doi.org/10.1016/j.ijthermalsci.2006.07.012>.
16. C. R. KHARANGATE and I. MUDAWAR, "Review of Computational Studies on Boiling and Condensation," *Int. J. Heat Mass Transfer*, **108**, 1164 (May 2017); <https://doi.org/10.1016/j.ijheatmasstransfer.2016.12.065>.
17. Y. SATO and B. NIČENO, "A Sharp-Interface Phase Change Model for a Mass-Conservative Interface Tracking Method," *J. Computat. Phys.*, **249**, 127 (Sep. 2013); <https://doi.org/10.1016/j.jcp.2013.04.035>.
18. J. U. BRACKBILL, D. B. KOTHE, and C. ZEMACH, "A Continuum Method for Modeling Surface Tension," *J. Comput. Phys.*, **100**, 2, 335 (1992); [https://doi.org/10.1016/0021-9991\(92\)90240-Y](https://doi.org/10.1016/0021-9991(92)90240-Y).
19. A. MUKHERJEE and S. G. KANDLIKAR, "Numerical Study of Single Bubbles with Dynamic Contact Angle During Nucleate Pool Boiling," *Int. J. Heat Mass Transfer*, **50**, 1–2, 127 (2007); <https://doi.org/10.1016/j.ijheatmasstransfer.2006.06.037>.
20. A. SIDDIQUE et al., "Study of Bubble Growth and Microchannel Flow Boiling Heat Transfer Characteristics Using Dynamic Contact Angle Model," *Thermal Sci. Eng. Prog.*, **20**, 100743 (2020); <https://doi.org/10.1016/j.tsep.2020.100743>.
21. E. MERLE et al., *Preliminary Design Assessment of the Molten Salt Fast Reactor* (2012).
22. M. S. SOHAL et al., *Engineering Database of Liquid Salt Thermophysical and Thermochemical Properties* (Mar. 2010); <https://doi.org/10.2172/980801>.
23. E. CERVI et al., "Development of a Multiphysics Model for the Study of Fuel Compressibility Effects in the Molten Salt Fast {Reactor},," *Chem. Eng. Sci.*, **193**, 379 (Jan. 2019); <https://doi.org/10.1016/j.ces.2018.09.025>.
24. A. TOMIYAMA et al., "Transverse Migration of Single Bubbles in Simple Shear Flows," *Chem. Eng. Sci.*, **57**, 11, 1849 (June 2002); [https://doi.org/10.1016/S0009-2509\(02\)00085-4](https://doi.org/10.1016/S0009-2509(02)00085-4).